Supporting Information

Reduced Bimolecular Recombination in Blade-Coated, High-Efficiency, Small-Molecule Solar Cells

Sebastian Engmann, Hyun Wook Ro, Andrew A. Herzing, Dean M. DeLongchamp, Chad R. Snyder, Lee J. Richter,
Material Measurement Laboratory, National Institute of Standards and Technology, Gaithersburg, MD 20899

Adam Barito, David J. Gundlach, Physical Measurement Laboratory, National Institute of Standards and Technology, Gaithersburg, MD 20899

Additional J(V)-Data

Table S 1 – Solar cell parameter of thin and thick p-DTS(FBTTh$_2$)$_2$: PC$_{71}$BM solar cells under AM 1.5 conditions. The data corresponds to the *J(V)*-curves shown in Figure 2 of the main manuscript. Each parameter is the average of at least 3 devices, the error bar corresponds to ± 2σ. Additionally, the best device performance ("Hero"-device) is given in brackets.

	Approx. thickness [nm]	Jsc [mA/cm2]	Voc [mV]	FF [%]	PCE [%]
BHJ w/o DIO as-cast	74	9.14 ± 1.03 (9.72)	835 ± 7 (835)	38.5 ± 10.1 (44.2)	3.0 ± 1.1 (3.5)
	250	5.96 ± 2.79 (6.95)	798 ± 8 (799)	34.3 ± 8.1 (37.2)	1.7 ± 1.2 (2.1)
BHJ w/ 0.3% DIO	80	10.70 ± 1.46 (10.6)	793 ± 153 (832)	43.8 ± 19.2 (54.8)	3.7 ± 1.9 (4.8)
	250	11.64 ± 0.72 (11.4)	818 ± 9 (814)	32.1 ± 8.7 (37.6)	3.0 ± 0.6 (3.5)
BHJ w/o DIO, after SVA	106	12.76 ± 0.49 (13.1)	765 ± 4 (768)	69.2 ± 8.8 (73)	6.8 ± 1.0 (7.4)
	250	16.13 ± 2.02 (17.3)	741 ± 9 (747)	66.9 ± 1.2 (67.5)	8.0 ± 1.3 (8.7)

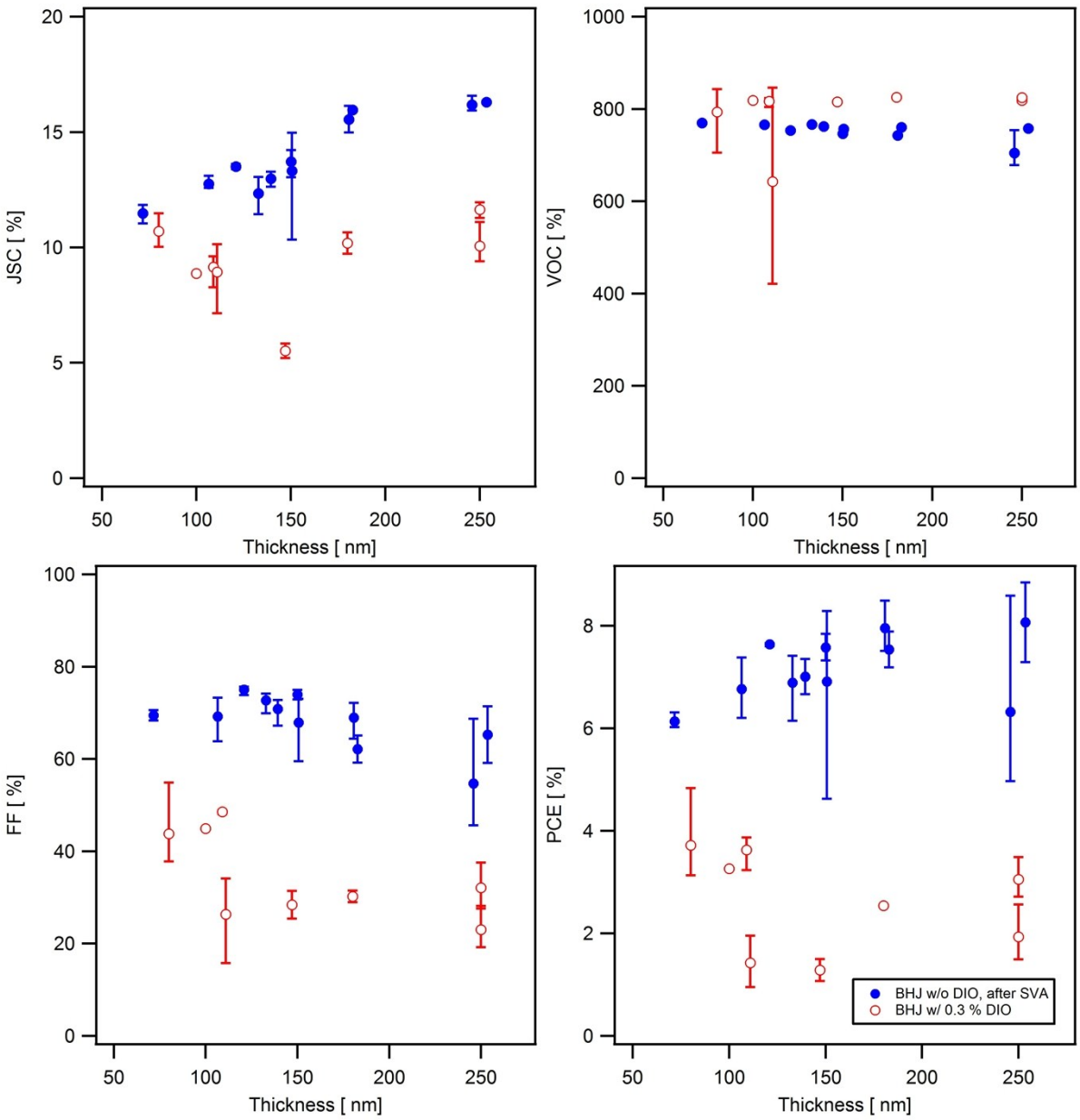

Figure S 1 - Solar cell parameter as function of active layer thickness of p-DTS(FBTTh$_2$)$_2$: PC$_{71}$BM solar cells under AM 1.5 conditions. Shown are the solvent vapor annealed BHJ w/o DIO and the BHJ processed from a 0.3 % DIO containing solution coated at 40 °C and dried at 80 °C for 5 min. Each parameter is the average of at least 3 devices. Error bars correspond to the best and worst device for that preparation condition.

Additional AFM images

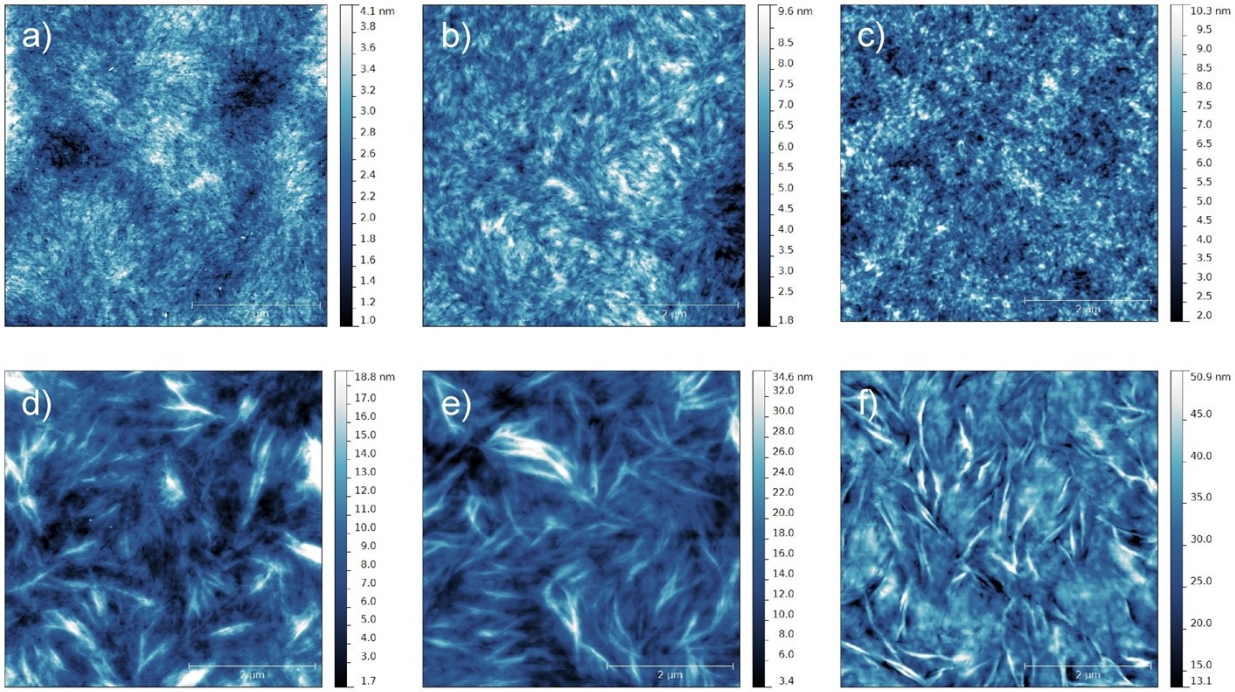

Figure S 2 - Atomic force microscopy (AFM) height images of p-DTS(FBTTh$_2$)$_2$: PC$_{71}$BM films cast from solutions without (a-c) and with (d-f) the addition of DIO. Shown are as-cast films (a, d), after thermal annealing (b, e), and after solvent annealing with THF (c, f). The dimensions of all images are (5 x 5) um.

Grazing Incidence X-Ray Diffraction (GIXD)

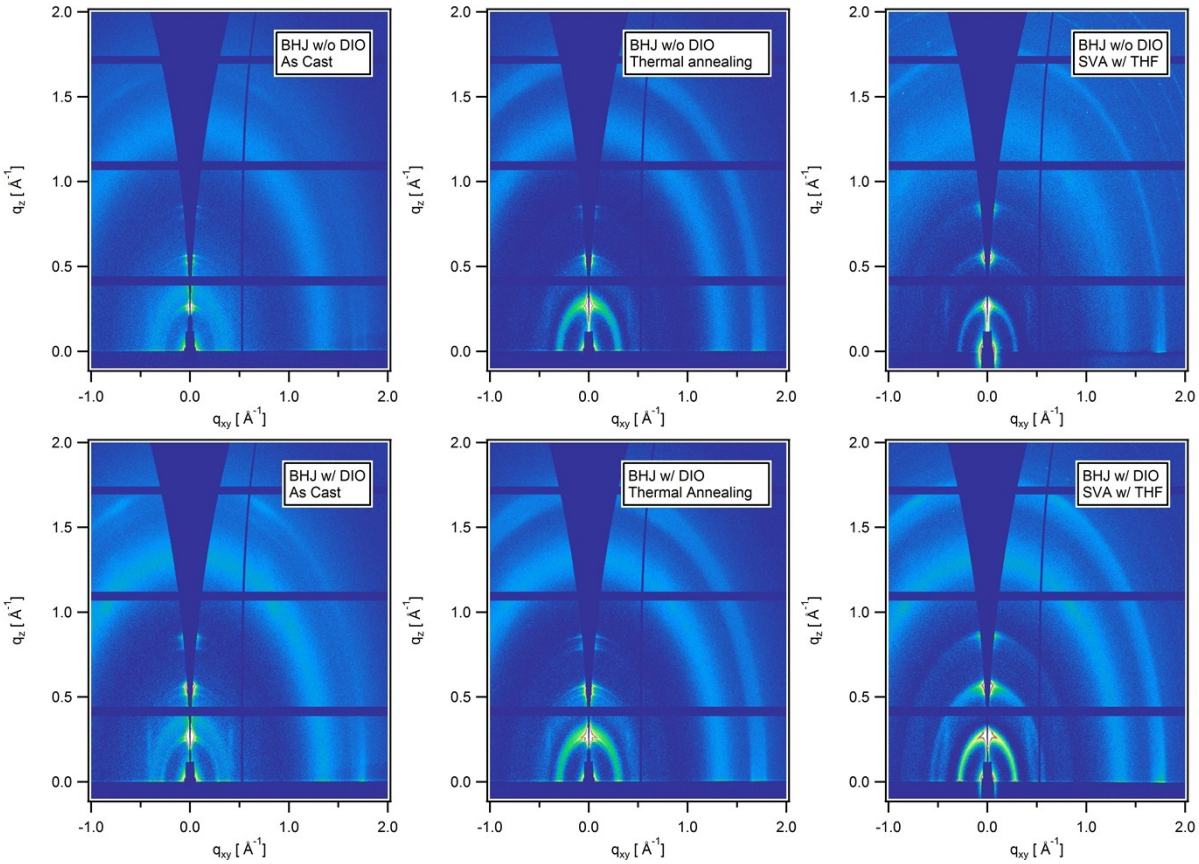

Figure S 3 - GIXD Detector images for p-DTS(FBTTh$_2$)$_2$: PC$_{71}$BM BHJs blade-coated from additive free (BHJ w/o DIO) and additive containing (DIO SA BHJ) solutions. From left to right, as cast, thermal annealing 5 min at 80 °C, solvent vapor annealing w/ THF.

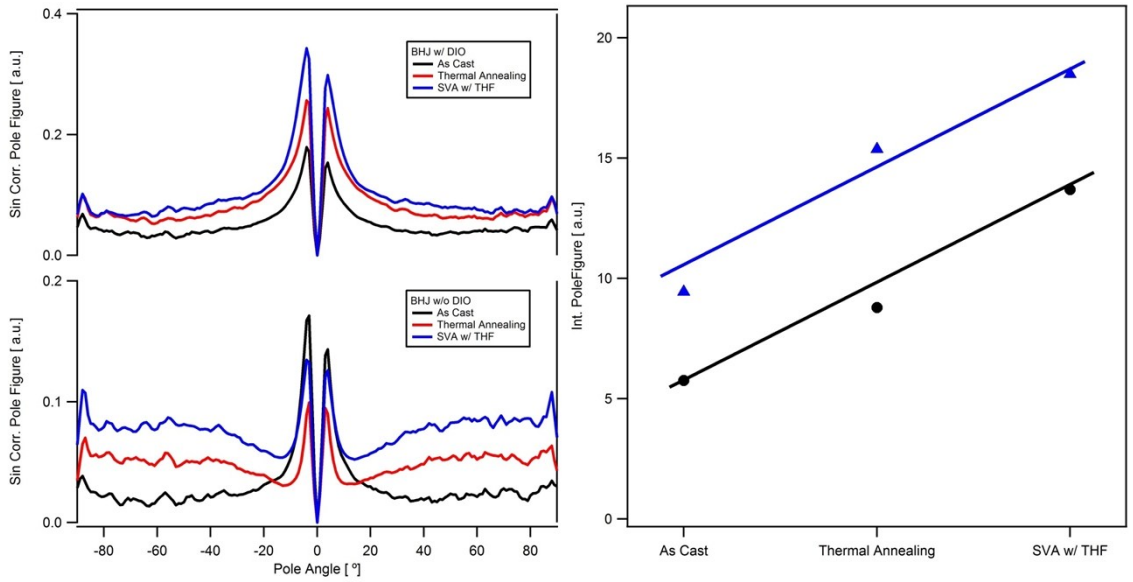

Figure S 4 - Corrected (001) pole figures and integrated pole figure values for 250 nm thick BHJs containing DIO and additive free. Shown are as-cast, thermal annealed and solvent vapor annealed films. Data were normalized with respect to the probed volume. Lines are guide to the eyes.

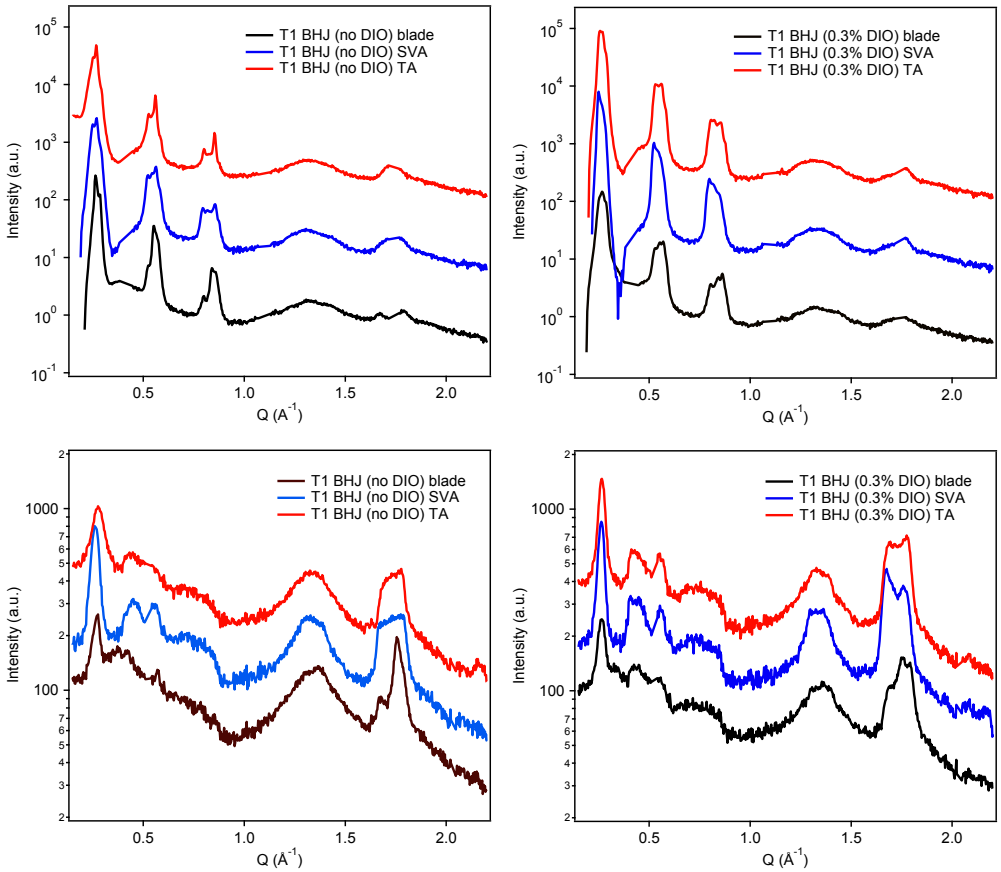

Figure S 5 - Line profile of the out-of-plane diffraction (top) and in-plane diffraction (bottom). Shown are data from 250 nm thick additive free films (left) and additive containing BHJs (right). TA refers to thermally annealed films, SVA to solvent annealed films. Additionally, shown are as-bladed films. The angle of incidence was 0.16°.

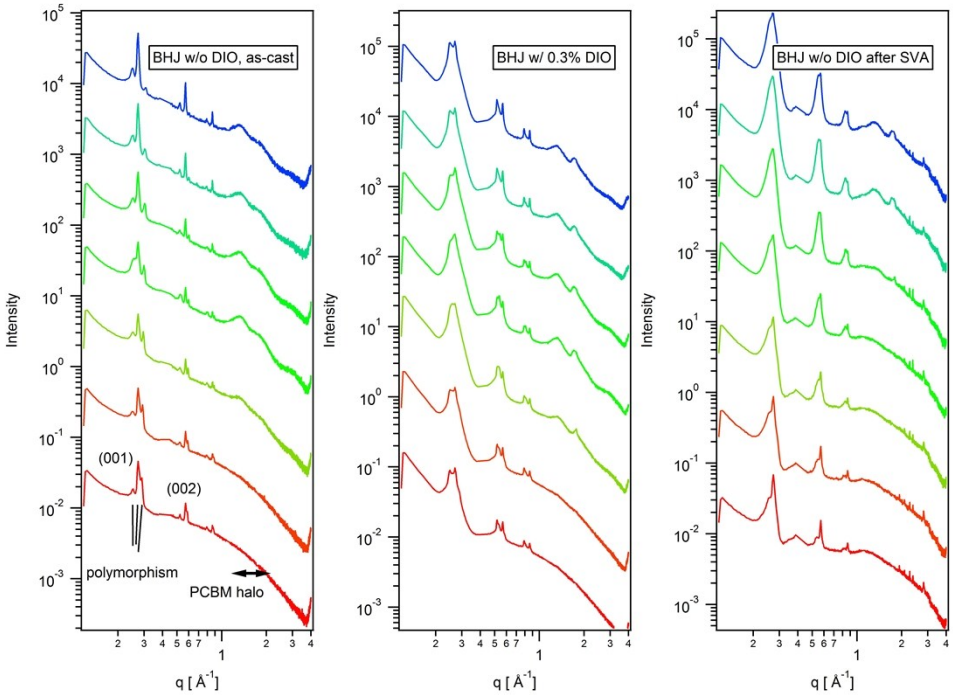

Figure S 6 – Line profile of the Out of Plane diffraction from 250 nm thick additive free films (left), additive containing BHJs (middle) and SVA annealed BHJs (right). The profiles are offset for clarity by multiples of 10. The angle of incidence was varied between 0.08° (red) and 0.20 ° (blue) in 0.02° steps. Note the distinct splitting of the (200) and (300) features due to multiple polymorphs.

Near edge X-ray absorption fine structure (NEXAFS)

NEXAFS spectroscopy was performed at the NIST/Dow soft X-ray materials characterization facility (beam line U7A) at the National Synchrotron Light Source (NSLS) of Brookhaven National Laboratory. The orientation of the small molecule at the interface was characterized by collecting carbon K-edge spectra in partial electron yield (PEY) mode with a grid bias of -50 V, corresponding to a surface-weighted sampling depth of ≈ 6 nm. The experimental standard uncertainty in the peak position for PEY spectra was 0.15eV; the yield uncertainty was 2 %. Five incident angles α (with respect to the surface plane) between 20° and 70° were chosen. The 1s-1π* resonance intensity was determined by fitting a Voigt function to the peak near 285 eV and dividing the peak area by the signal intensity at 330 eV, which is an orientation insensitive measure of the carbon atom density within the sampling volume. The intensities, thus normalized, were then fit to $\sin^2\alpha$. This linear fit was used to extrapolate intensities at 0 and 90° incidences, which were then used to calculate the figure of merit. Allowing for non-idealities in the polarization state of the X-ray beam (fraction p-polarized P), R can be expressed as:

$$R = \frac{I(90°) - I(0°)}{I(90°) + I(0°)} = \frac{P\left(1 - 3\left\langle \cos^2\theta \right\rangle\right)}{2\left(1 - \left\langle \cos^2\theta \right\rangle\right) - P\left(1 - 3\left\langle \cos^2\theta \right\rangle\right)},$$

where θ is the tilt of the transition dipole vector from the surface normal, <...> is an average over the orientation distribution. Ideally, the figure of merit R would be -1 for pure face-on order and 1 for pure edge-on order; however, due to P = 0.85, the limiting value for edge-on order is found to be 0.7. For an isotropic distribution ($\langle\cos^2\theta\rangle$ = 1/3), R is 0.

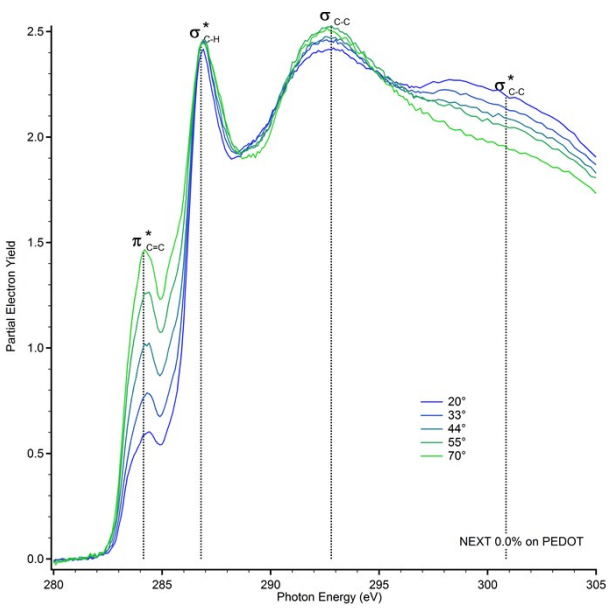

Figure S7 - Surface NEXAFS spectra for various incident angles. The film was a BHJ film in the additive free case.

Table S1 - Summary of the NEXAFS Results. Volume percentage of PCBM at the film surface, Figure of merit R = [I(90)-I(0)] / [I(90) + I(0)] for the 1s-1π^* and 1s-1σ^* transition and the approximated tilt of the transition dipole vector, corresponding to the 1s-1π^* transition, with respect to the surface normal θ.

	[70]PCBM [%]	$R(\pi^*)$	$R(\sigma^*)$	θ [°]
BHJ 0.0%	0.03	0.56 ± 0.02	-0.13 ± 0.01	15
BHJ 0.3%	0.00	0.45 ± 0.03	-0.10 ± 0.01	20
BHJ 0.6%	0.00	0.52 ± 0.02	-0.14 ± 0.01	17
BHJ 1/0%	0.00	0.33 ± 0.02	-0.06 ± 0.00	24
Neat 0.0%	x	0.31 ± 0.01	-0.08 ± 0.01	25
Neat 0.3%	x	0.56 ± 0.02	-0.13 ± 0.01	15
Neat 0.6 %	x	0.46 ± 0.01	-0.09 ± 0.00	20
Neat 1.0%	x	0.38± 0.01	-0.08 ± 0.00	23

TEM cross section of DIO containing film

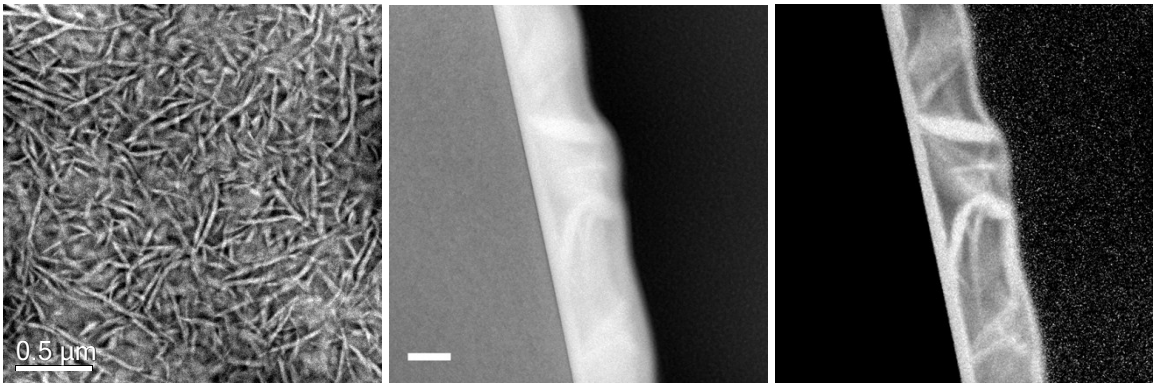

Figure S8 - TEM images of a BHJ cast from solution containing 1% DIO. Low-loss EFTEM ratio image of a plan-view specimen (left), zero-loss filtered bright field image (middle) and low-loss ratio of the plasmonic response of the same section (right). The film was cast on a silicon substrate with natural oxide and thin (approx. 30 nm) PEDOT:PSS layer. Small molecule domains appear brighter compared to PCBM rich regions. The scale bars are 0.5 µm and 100 nm for the plan-view and cross-section images, respectively.

Grazing Incidence Small Angle X-Ray Scattering (GISAXS)

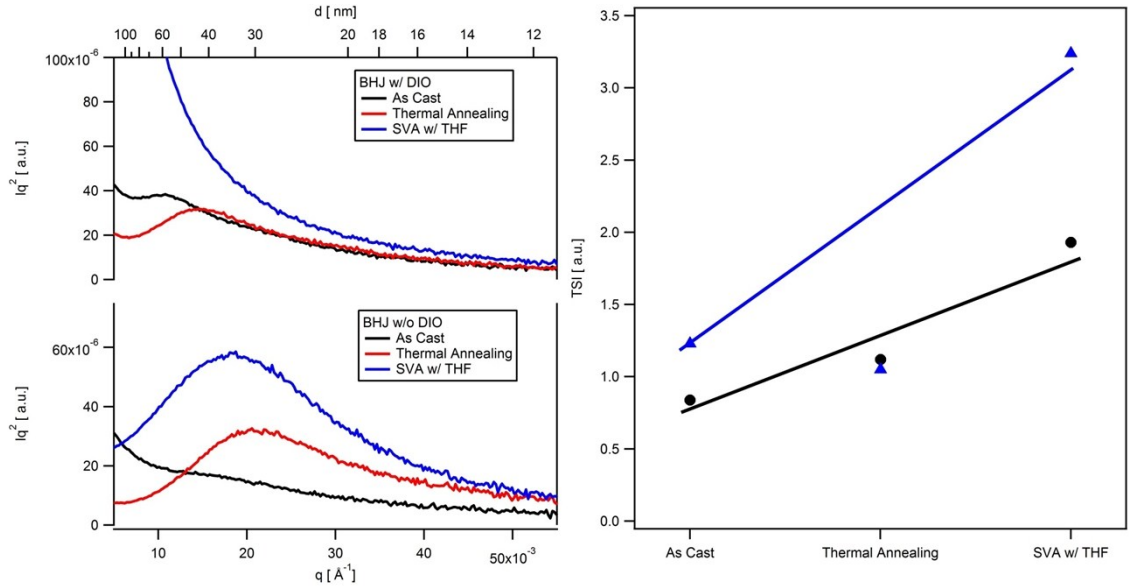

Figure S 9 – Iq² of the scattering intensity obtained near the sample horizon ($q_z \approx 0$, left). Integrated scattering invariant obtained from an integration of q^2-weighted diffraction intensity $ISI = \int I(q)q^2 dq$ (right).

In Ref [1], characteristic lengths scales were derived by fitting Iq^2 data to a lognormal function, and extracting both the peak d_{max} and arithmetic mean d_{EW}, reciprocal dimensions. We duplicate this analysis for the blade-coated films below, to allow direct comparison.

Fit to LogNormal - Results

	"Neat" BHJ			DIO SA BHJ		
	As-bladed	TA	SVA	As-bladed	TA	SVA
d_{max} [nm]	34.3 ± 11.7	29.0 ± 0.9	41.0 ± 11.4	50.1 ± 10.6	37.1 ± 6.3	26.5 ± 0.3
d_{EW} [nm]	16.6 ± 6.2	23.0 ± 1.9	24.4 ± 1.8	27.7 ± 7.6	29.1 ± 6.1	21.4 ±0.8

Table 2 - Characteristic length scales within BHJ cast without and with DIO as obtained from a fit of the q^2 weighted scattering intensity to a log-normal distribution with constant offset, d_{max} length scale at which the lognormal distribution reaches its maximum value, d_{EW} to the position of the arithmetic mean of the lognormal distribution. Shown are the results for as-bladed films, after 5 min thermal annealing at 80 °C (TA), as well after 120 s solvent vapor annealing with THF (SVA). Error bars correspond to the average of 4 samples.

Electrical Characterization – Additional / Intermediate Impedance Results

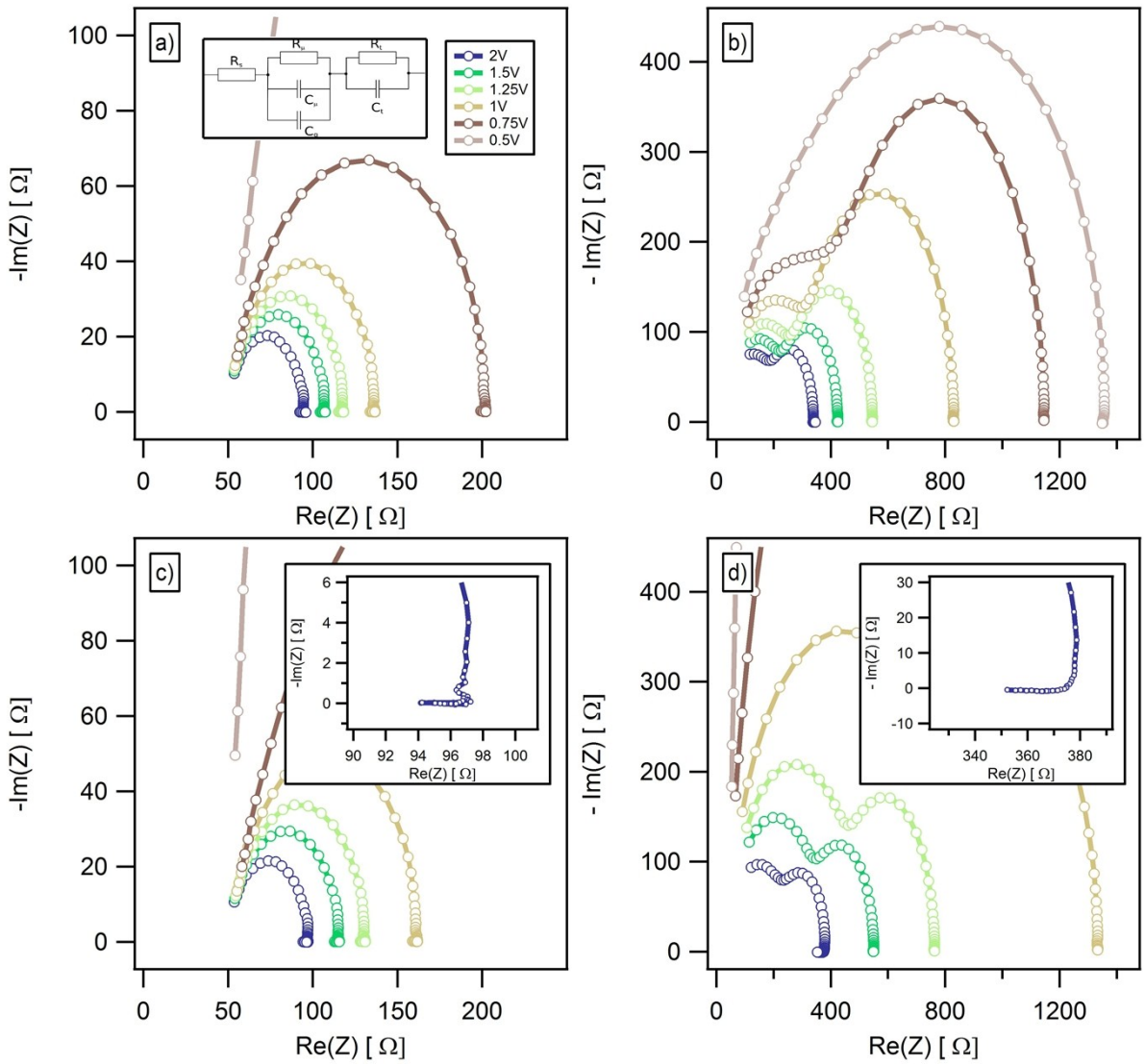

Figure S 10 - Selected Nyquist-plots of the bias dependent impedance data obtained on a BHJ after SVA (a,c) and a BHJ cast from a solution containing 0.3 % DIO (b,d). Shown data was obtained under (1sun) illumination (a,b) as well as under dark (c,d) conditions, in the frequency range 20 Hz to 2 MHz. Also shown in a) is the equivalent circuit model used for the impedance analysis of the BHJ after SVA.

Electrical Characterization – Discussion of Negative Capacitance (NC)

For organic light emitting diodes (OLEDs) devices Pingree, et al. attributed this region to an mobility increase with increasing bias and observed, in agreement with Poole-Frenkel theory, that the onset of the NC region increases exponentially with the square root of the applied bias.[2] Shown in Figure S 11 is the frequency dependence of the onset of negative capacitance for the DIO SA BHJ as function of the applied bias voltage. For the bias range studied we observe a similar exponential dependence as reported by Pingree, for both the

illuminated and non-illuminated DIO SA BHJ device. In case of illumination a shift towards smaller frequencies for the same bias can be observed, while maintaining the same barrier height (slope). We interpret this as saturation of trap states upon illumination by photogenerated charge carriers. We want to suggest two possibilities as the origin of the trap levels, the first one might be residual or decomposed DIO, the second one might be due to grain boundaries formed during the excessive crystal growth of the small molecule donor. However, these are mere suggestions and cannot be revealed via impedance measurement. For applied biases below 1.5 V we were not able to resolve the NC region, and the data is dominated by the low frequency arc. In case of the solvent vapor annealed device, the NC region was comparably less pronounced than in the DIO case and noise levels prohibited analysis.

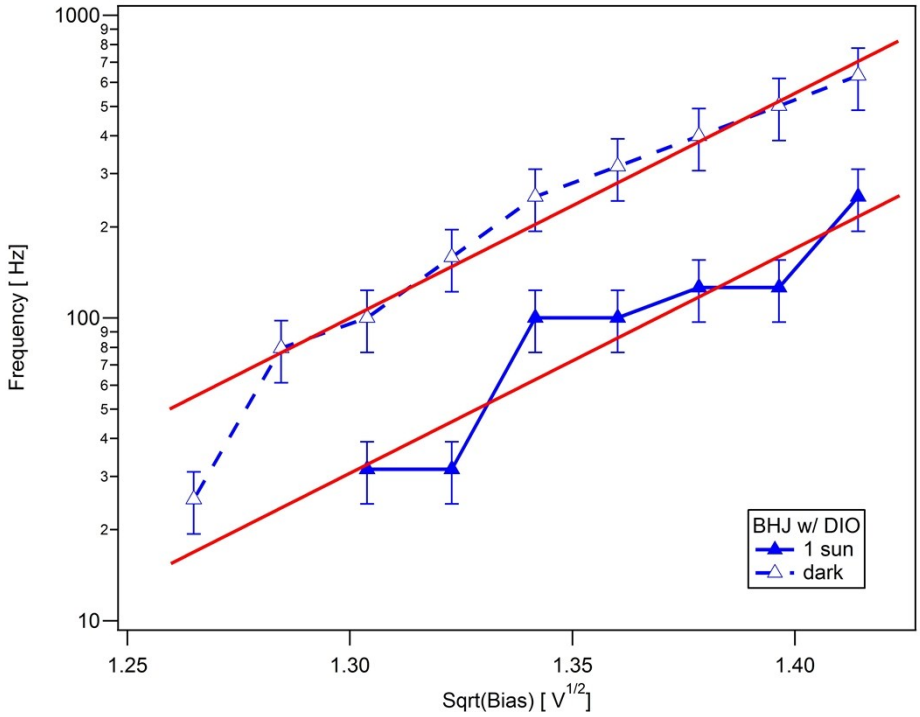

Figure S 11 - Frequency dependence of the intersection *Im(Z)* = 0 as function of the square root of the applied bias for the BHJ w/DIO device under and without illumination. Error bars correspond to the uncertainty of the zero crossing based on a linear fit of adjacent points. Lines are guides to the eye.

Fit of Impedance data and extraction of other device parameters

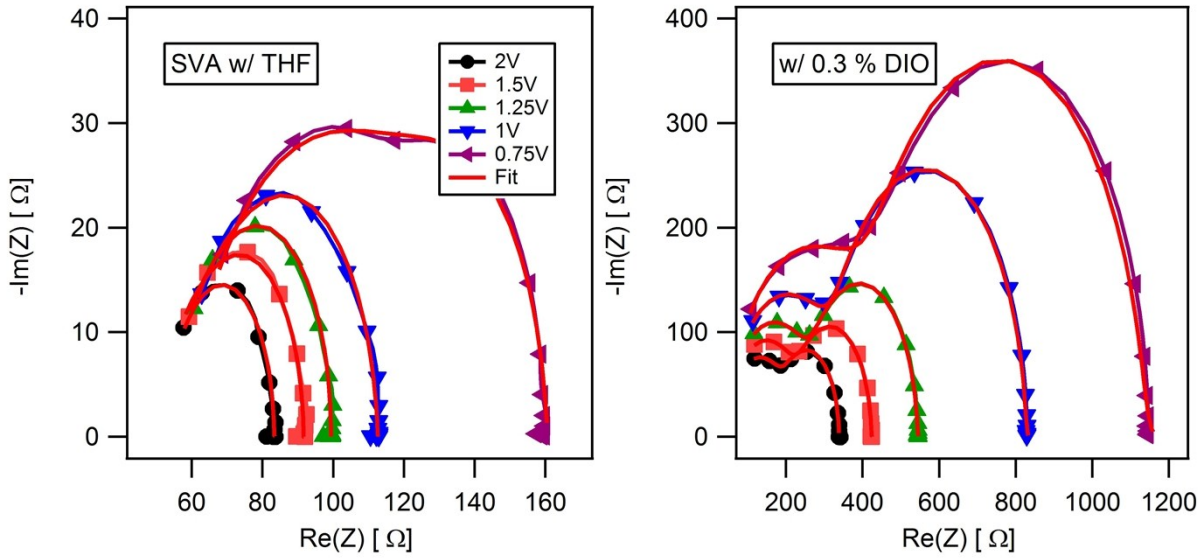

Figure S 12 – Selected Nyquist plots and fits using the in the main manuscript described equivalent circuit. (Left) Solvent vapor annealed BHJ and (Right) DIO SA BHJ.

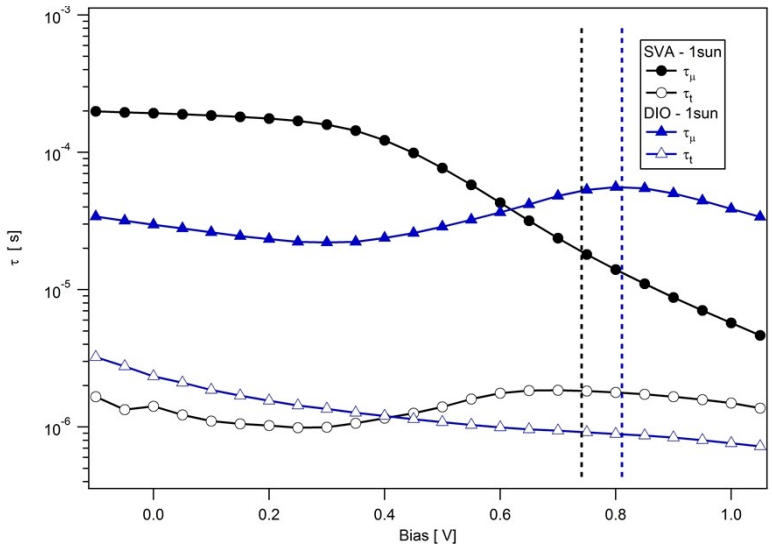

Figure S 13– The two RC time constants extracted from a fit to the experimental data of the BHJ after SVA and for the DIO SA BHJ. Indicated via vertical broken lines are the respective open circuit voltages under 1 sun illumination.

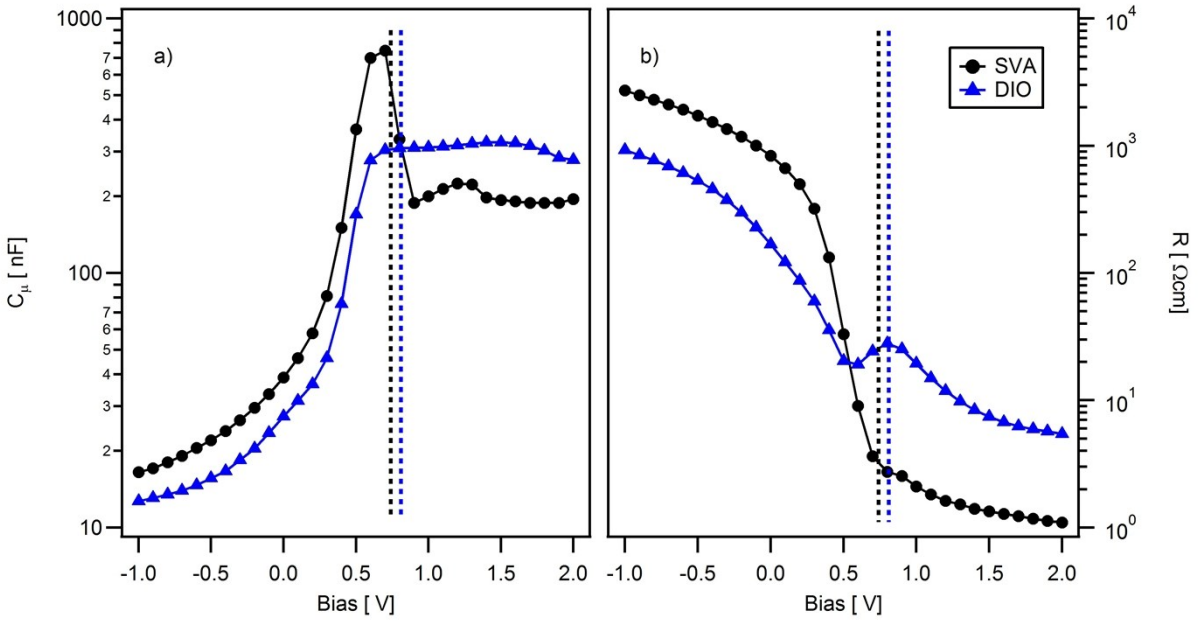

Figure S 14 – (a) Chemical capacitance C_μ and (b) recombination resistance R_μ as function of the applied for the solvent vapor annealed BHJ and DIO SA BHJ.

Fit of the *J(V)*-curve in order to determine the proportionality constant α

For efficient cells, high fill factors and shunt resistances, it was found that the charge carrier generation rate within the device is nearly field independent and as such the *J*(*V*)-curve can be estimated using the easily measureable short circuit current density J_{sc} and the recombination rate [3]

$$J(V) \approx -J_{SC} + qLR(V) \qquad \text{(S1)}$$

With $R \approx \frac{n}{\tau_\mu(n)}$ and $n = \frac{1}{L}\int C_\mu dE_f + n_0 = \frac{1}{qL}\int C_\mu \alpha \, dV + n_0$

Shown in the figure below is a fit of the experimentally determined J(V)-curve under 1-sun illumination of the SVA annealed BHJ and a fit using the equations above and via impedance determined chemical capacitance and charge carrier lifetime. The fit yields an α = 0.16

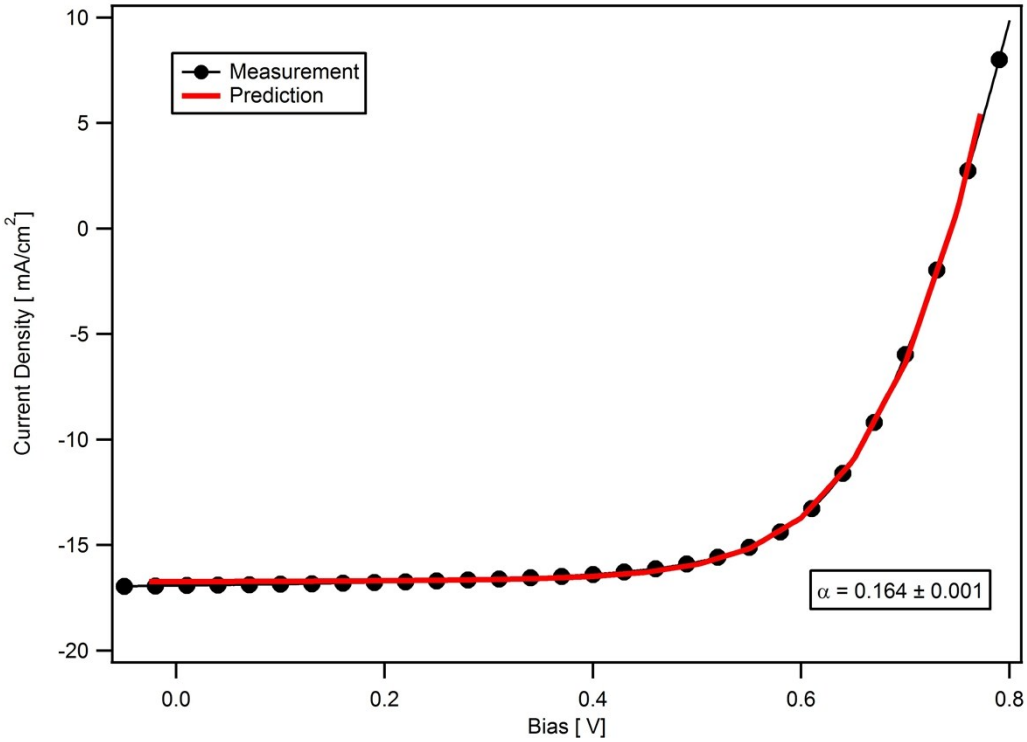

Figure S 15 – Fit of the *J(V)*-characteristics using Eq. (S1).

References

[1] S. Mukherjee, X. Jiao, and H. Ade, "Charge Creation and Recombination in Multi-Length Scale Polymer:Fullerene BHJ Solar Cell Morphologies," *Advanced Energy Materials,* vol. 6, pp. n/a-n/a, 2016.

[2] L. S. C. Pingree, B. J. Scott, M. T. Russell, T. J. Marks, and M. C. Hersam, "Negative capacitance in organic light-emitting diodes," *Applied Physics Letters,* vol. 86, p. 073509, 2005.

[3] J. I. Basham, T. N. Jackson, and D. J. Gundlach, "Predicting the J–V Curve in Organic Photovoltaics Using Impedance Spectroscopy," *Advanced Energy Materials,* vol. 4, pp. n/a-n/a, 2014.